

Lateral resistance of polyurethane-reinforced ballast with the application of new bonding schemes

Laboratory tests and discrete element simulations

Jing, Guoqing; Zhang, Xu; Jia, Wenli

DOI

[10.1016/j.conbuildmat.2019.06.114](https://doi.org/10.1016/j.conbuildmat.2019.06.114)

Publication date

2019

Document Version

Accepted author manuscript

Published in

Construction and Building Materials

Citation (APA)

Jing, G., Zhang, X., & Jia, W. (2019). Lateral resistance of polyurethane-reinforced ballast with the application of new bonding schemes: Laboratory tests and discrete element simulations. *Construction and Building Materials*, 221, 627-636. <https://doi.org/10.1016/j.conbuildmat.2019.06.114>

Important note

To cite this publication, please use the final published version (if applicable).
Please check the document version above.

Copyright

Other than for strictly personal use, it is not permitted to download, forward or distribute the text or part of it, without the consent of the author(s) and/or copyright holder(s), unless the work is under an open content license such as Creative Commons.

Takedown policy

Please contact us and provide details if you believe this document breaches copyrights.
We will remove access to the work immediately and investigate your claim.

1 **Lateral resistance of polyurethane-reinforced ballast with the**
2 **application of new bonding schemes: laboratory tests and discrete**
3 **element simulations**

4
5 Guoqing Jing^a, Xu Zhang^{b,*} & Wenli Jia^c
6

7 ^a School of Civil Engineering, Beijing Jiaotong University, Beijing 100044, China

8 ^b School of Civil and Transportation Engineering, Guangdong University of Technology, Guangzhou 510006,
9 China

10 ^c Faculty of Civil Engineering and Geosciences, Delft University of Technology, Delft, 2628CN, Netherlands

11

12 * Corresponding author, e-mail: xuzhang@gdut.edu.cn

13

14 **Abstract:** To mitigate the ballast flight risk in the high-speed railway, this paper presents three new polyurethane
15 bonding schemes which have negligible influence to tamping operations. With the application of these bonding
16 schemes, a series of laboratory tests indicated that the polyurethane-reinforced ballast exhibited much larger
17 lateral resistance than the ordinary ballast by 31% at least. Discrete element simulation results further
18 demonstrated that the polyurethane improved the load-bearing capacity of the ballast at the particle scale through
19 effectively restraining the particle movement. Therefore, the proposed bonding schemes ensure adequate lateral
20 ballast resistance and are effective measures for improving the ballast performance.

21

22 **Key words:** high-speed railway; ballast; polyurethane; discrete element method; lateral resistance; single sleeper
23 pull-out test

24

25 **1. Introduction**

26 Railway ballast is often constructed using crushed stones and works as an important granular layer
27 under the track superstructure. One of the main functions of the ballast layer is to provide sufficient
28 lateral resistance to the track panel so that the track geometry and stability can be kept and the train
29 running safety can be ensured. Insufficient lateral ballast resistance may lead to some
30 serious problems such as excessive movement of the track panel and track lateral buckling [1]. In
31 order to provide enough lateral ballast resistance to the track, numerous measures have been taken
32 all over the world to reinforce the ballast especially since the extensive application of the
33 continuously welded rail (CWR) track which requires large lateral ballast resistance to prevent
34 the track from bulking [2-6]. Among these measures, increasing the height of the shoulder
35 ballast to be 100-150 mm over the ballast surface is considered as an effective way in China and
36 many other countries for years.

37 However, with the rapid development of the high-speed railways over the past few years, the
38 high shoulder ballast brings a new problem. It was reported that the shoulder ballast stones may fly
39 due to the strong wind caused by the high-speed trains, and this phenomenon becomes a severe
40 problem in the railways whose design speed reaches or exceeds 350 km/h [7,8]. Except for the
41 shoulder ballast, the surface ballast stones near the sleeper centre also may fly easily due to the
42 strong negative air pressure formed under the high-speed train bogies [7,9]. The ballast stones
43 blowing up from the track during the train passage would probably strike the train components and
44 the rail heavily which further results in failure or damage problems to the train and the rail [10].
45 From the perspective of mitigating the ballast flight due to the high speed running of the trains, the
46 height of the shoulder ballast should be decreased just as the flat ballast shoulder adopted in
47 European railways. But regarding that the shoulder and crib ballast play important roles in the
48 lateral ballast resistance [11], decreasing the height of the shoulder ballast will reduce the lateral
49 ballast resistance to some extent though it is indeed helpful in mitigating the ballast flight. When the
50 shoulder ballast height is decreased, other measures should be taken to gain enough lateral ballast
51 resistance.

52 Aiming at this issue, the polyurethane, a kind of polymer material, has been applied to reinforce
53 the ballast in recent years by bonding the granular ballast particles as a massive structure. To
54 investigate the mechanical properties and performance of the polyurethane-reinforced ballast, a few
55 laboratory and field tests have been conducted by researchers. According to the triaxial test results,
56 Lee et al. [12] figured out that both the shear strength and the elastic moduli of the
57 polyurethane-mixed ballast increase linearly with the content of the polyurethane. Woodward et al.
58 [13-15] and Kennedy et al. [16] reported laboratory tests and engineering practices to show the
59 applications of the polyurethane to help maintain track geometry and absolute clearances, to

60 improve the ballast stiffness and to reduce the ballast settlement. Woodward et al. [17] and
61 Kruglikov et al. [18] presented that the lateral resistance of the ballast increased remarkably after
62 the shoulder ballast was reinforced with the polyurethane along the longitudinal direction to form a
63 block wall at the track side. Thomas et al. [19] demonstrated an application of the polyurethane to
64 obtain more uniform load distribution of the ballasted track on a masonry bridge. These studies
65 demonstrate that the polyurethane has been successfully applied to reinforce the railway ballast for
66 many different goals. The relevant test results and engineering practices indicate that the application
67 of the polyurethane really improves the ballast performance effectively.

68 Focusing on mitigating the ballast flight risk in high-speed railways, the polyurethane is often
69 sprayed across the whole ballast surface. Fig. 1 illustrates the sketch of the widely adopted bonding
70 scheme. Since all the particles from the surface to a certain depth in the ballast layer are strongly
71 bonded by the polyurethane, this bonding scheme is effective in avoiding the ballast flight even in
72 the cases when the trains run at very high speeds. However, this bonding scheme has an obvious
73 disadvantage of affecting the tamping operations significantly. Because when all the surface ballast
74 particles are entirely bonded with the polyurethane, it is quite difficult to insert the arms of the
75 tamping machines into the bonded ballast to a required depth. New bonding schemes that can avoid
76 the ballast flight and have negligible influence to the tamping operations simultaneously are very
77 desirable for reinforcing the ballast in the high-speed railways. Meanwhile, although lots of studies
78 have proved that it is effective to reinforce the ballast with the polyurethane, the mechanisms that
79 how the polyurethane affects the micro-mechanical behaviours of the ballast have not been revealed
80 yet, which still needs further insightful research.

81 **2 New bonding schemes for reinforcing the ballast with polyurethane**

82 This paper proposes three new bonding schemes, denoted as E, C & B, respectively, for reinforcing

83 the high-speed railway ballast with the polyurethane. In these new bonding schemes, only the
84 ballast in four target regions instead of all the surface ballast are required to be bonded with the
85 polyurethane. Fig. 2 demonstrates the four target regions where the ballast shall be bonded. Among
86 these regions, two are at the sleeper ends and the other two are near the sleeper centre. In the
87 proposed bonding scheme E, the shoulder ballast near the two sleeper ends are required to be
88 bonded. In the bonding scheme C, the crib ballast near the sleeper centre shall be bonded, and in the
89 bonding scheme B, both the ballast in the sleeper end and centre areas are required to be bonded.

90 | Since the target regions in Fig. 2 almost cover all the dangerous areas where the ballast flight is
91 likely to occur, the new bonding schemes meet the requirement of avoiding the ballast flight by
92 bonding the particles in these dangerous regions with the polyurethane. In the meantime, the new
93 bonding schemes do not require the application of the polyurethane to the ballast in the areas near
94 the rails where the tamping machines always work. Hence, the new bonding schemes have
95 negligible influence to the tamping operations to the ballast. It is also worthy being noted that as
96 indicated by the dimensions in Fig. 2, the target bonding regions in the three new bonding schemes
97 are just 18.1%, 7.2%, and 25.3%, respectively, of the whole ballast surface, which can help reduce
98 the dosage of the polyurethane distinctly. Also, with the new bonding schemes, the height of the
99 ballast shoulder can be decreased, which reduces the dosage of the ballast material. Therefore,
100 relative to the conventional bonding scheme, the new bonding schemes are more economical in the
101 dosage of the ballast and the polyurethane material. In a word, the proposed bonding schemes
102 simultaneously have multiple advantages of avoiding the ballast flight, reducing the dosage of the
103 polyurethane and having negligible influence to the tamping operation.

104 However, the new bonding schemes have much smaller bonding area than the conventional
105 scheme, and the ballast shoulder height is cancelled, both of which bring about a problem that

106 whether the lateral resistance of the ballast locally reinforced with the polyurethane based on the
107 new bonding schemes is enough to keep the track lateral stability or not? Aiming at this issue,
108 laboratory tests and discrete element simulations were carried out in this paper to investigate the
109 lateral resistance of the ballast locally reinforced with the polyurethane based on the proposed
110 bonding schemes. Two different bonding depth of 200 mm and 300 mm in the ballast were studied
111 in the tests to investigate the feasibility of the new bonding schemes in providing enough lateral
112 resistance for the high-speed railway track. Furthermore, the discrete element method (DEM) was
113 employed in this paper to study the micro-mechanical behaviours of the ballast reinforced with the
114 polyurethane since the DEM has the advantage in simulating the mechanical behaviours of granular
115 materials. The mechanism that how the polyurethane materials helps increase the lateral ballast
116 resistance was also studied and revealed through the DEM analyses.

117 **3 Laboratory tests on the lateral resistance of polyurethane-reinforced ballast**

118 The single sleeper pull-out test (SSPT) is an effective and frequently used method to evaluate the
119 ballast resistance. In order to evaluate the lateral resistance of the ballast locally reinforced with the
120 polyurethane, a series of laboratory tests were carried out using a full-scale test track and will be
121 presented in this section.

122 ***3.1 Material properties of ballast and polyurethane***

123 The ballast material adopted in the test is basalt with the particle size gradation illustrated in Fig.
124 3, which meets the requirement of the ballast gradation standard in China. The polyurethane
125 material utilized in this test was jointly developed by Beijing Jiaotong University and State Key
126 Laboratory of Special Functional Waterproof Materials (SKLSFWM) in China. The polyurethane
127 was produced by mixing two components, namely the component A-isocyanate & the component

128 B-polyols, with the volume ratio of 1:1. The strength of the produced polyurethane rapidly reaches
129 70% of its final strength one day after the mixing and continues to increase with the time. The
130 mechanical parameters of the polyurethane were measured in SKLSFWM and listed in Table 1.

131 **3.2 Test facility**

132 A full-scale test track comprising of sleepers and ballast was established in Beijing Jiaotong
133 University. The total length of the test track was 12 m. The thickness of the ballast under the sleeper
134 was 350 mm and the total width of the ballast bed was 3,600 mm. The width of the ballast shoulder
135 was 500 mm and the slope was 1:1.75. The dimensions of the test track were consistent with those
136 in the high-speed railway ballasted track in China.

137 The construction procedures of the test track are described hereinafter. Firstly, the ballast
138 material were compacted in four layers with an electronic plate compactor to form the dense ballast
139 bed. Then, the type IIIc pre-stressed concrete sleepers, which are frequently adopted for the
140 ballasted track in China's high-speed railways, were laid on top of the ballast with the spacing of
141 600 mm. After that, extra ballast material was put between the adjacent sleepers and at the sleeper
142 ends, and compacted in three layers to form the crib and shoulder ballast. Finally, the polyurethane
143 was sprayed from the top surface of the ballast using a specialized spray gun. The polyurethane then
144 went down into the ballast to form coating on the surface of the ballast particles and bond the
145 particles at the contacts.

146 Fig. 4 shows the photographs of the test track with and without the reinforcement of the
147 polyurethane. For each of the three proposed bonding schemes, two test tracks with different
148 bonding depth in the ballast, i.e. 200 mm and 300 mm, were constructed by controlling the dosage
149 of the polyurethane material. As a reference, two extra test tracks were constructed without the
150 reinforcement of the polyurethane. The summary of the laboratory tests that were carried out is

151 listed in Table 2. Among all the eight tests, the shoulder ballast height was only set in the test ‘Ns’,
152 which represents the typical ballasted track in China with the shoulder ballast height of 150 mm. By
153 comparing the results in the tests ‘Ns’ and ‘Nf’ that were carried out on the unreinforced ballast, the
154 effect of the shoulder ballast height on the lateral resistance can be studied. For the other six tests,
155 the first capital letters in their test names indicate the bonding scheme as discussed in Section 2 and
156 the numbers after the capital letters indicate the bonding depth is 200 or 300 mm.

157 ***3.3 Test apparatus and procedures***

158 A set of specialized apparatus consisting of an oil pump, a force transducer, a reaction frame,
159 two dial indicators and a data logger was developed and adopted to measure the lateral resistance
160 force of the ballast and the lateral displacement of the sleeper in the SSPT. Fig. 5 presents the
161 apparatus utilized for the measurement in the test.

162 In order to pull out the sleeper, the oil pump together with the force transducer and the reaction
163 frame was horizontally installed at one sleeper end. The dial indicators were fixed above the sleeper
164 with their pointers parallel to the sleeper. In the test, the oil pump was controlled to apply
165 multi-stage loads to the sleeper. When the sleeper moved slowly under the horizontal load, the
166 lateral force measured by the force transducer and the lateral displacement measured by the dial
167 indicators were collected and saved in the data logger. Each load stage continued until the sleeper
168 displacement increased to a stable value, and then the next stage of load was applied. Each test did
169 not stop until the state that the lateral resistance force of the ballast almost kept stable. After each
170 sleeper pull-out test, the test track including the ballast was dismantled and re-established with the
171 same method as described in Section 3.2 for the next test, which ensured close ballast densities in
172 all tests. Moreover, three repetitive tests were carried out for each test condition in Table 2. The
173 measured results of the three tests were averaged as the test result for that load condition, and will

174 be presented in the paper.

175 **3.4 Test results**

176 Fig. 6 illustrates the lateral resistance force F of the reinforced ballast as a function of the lateral
177 sleeper displacement d for the three new bonding schemes. In each subplot, the results of the tests
178 ‘Ns’ and ‘Nf’ are also presented for comparison. It can be found the resistance force increases
179 rapidly with the lateral sleeper displacement at the initial stage, and then gradually becomes stable
180 when the sleeper displacement continues to increase. The lateral resistance force in the test ‘Ns’ is
181 distinctly larger than that in the test ‘Nf’, which demonstrates the important contribution of the 150
182 mm shoulder height to the lateral ballast resistance.

183 It also can be seen that the lateral resistance forces of the reinforced ballast based on all the
184 three bonding schemes are remarkably larger than those in the tests ‘Ns’ and ‘Nf’. For the same
185 bonding scheme, the larger lateral resistance force was gained for the reinforced ballast with the
186 deeper bonding depth of 300 mm. These results indicate the application of polyurethane does result
187 in distinct increase to the lateral ballast resistance. Furthermore, the deeper the ballast is bonded
188 with the polyurethane, the larger is the lateral resistance of the reinforced ballast, which can be even
189 larger than that of the unreinforced ballast with the shoulder height of 150 mm.

190 The lateral resistance force at the sleeper displacement of 2 mm obtained in the single sleeper
191 pull-out test is always used for the quantitative evaluation of the lateral ballast resistance in
192 practical engineering. To further quantify the lateral ballast resistance in the tests, the resistance
193 forces at $d=2$ mm were collected from the measured results in Fig. 6 and listed in Table 3. The
194 relative differences between the lateral resistance forces of the reinforced ballast and those in the
195 tests ‘Ns’ and ‘Nf’ were also calculated and listed in the table. It can be found when the sleeper
196 displacement reached 2 mm, the resistance forces of the ballast were 10.02 kN and 7.05 kN,

197 respectively, in the tests ‘Ns’ and ‘Nf’. Apparently, without the ballast shoulder height, the lateral
198 resistance force of the ballast decreases by nearly 30%.

199 When the ballast particles near the sleeper ends were bonded with the polyurethane, the lateral
200 resistance force of the reinforced ballast with the bonding depth of 200 mm in the test ‘E2’
201 increased by 41% relative to the test ‘Ns’ and by 60% relative to the test ‘Nf’. With the deeper
202 bonding depth of 300 mm in the test ‘E3’, the lateral resistance force increased by 100% relative to
203 the test ‘Ns’, and by 128% relative to the test ‘Nf’.

204 When the ballast near the sleeper centre was reinforced with the polyurethane with the bonding
205 depth of 200 mm, the increase of the ballast lateral resistance force in the test ‘C2’ was 41% in
206 contrast to that in the test ‘Ns’ and was 60% comparing with that in the test ‘Nf’. With the deeper
207 bonding depth of 300 mm in the test ‘C3’, the lateral resistance force increased by 41% relative to
208 that in the test ‘Ns’, and by 100% relative to that the test ‘Nf’.

209 When both the ballast near the sleeper ends and the sleeper centre were simultaneously
210 reinforced with the bonding depth of 200 mm, the lateral resistance force in the test ‘B2’ increased
211 by 70% with respect to the test ‘Ns’ and by 142% with respect to the test ‘Nf’. When the bonding
212 depth was 300 mm, the ballast resistance in the test ‘B3’ increased by 100% with respect to the test
213 ‘Ns’ and by 184% with respect to the test ‘Nf’.

214 Obviously, the lateral resistance force increased by 31% at least in the tests when the ballast was
215 reinforced with the polyurethane with the application of the three new bonding schemes. The lateral
216 resistance force of the reinforced ballast in the test ‘C2’ with the bonding depth of 200 mm was the
217 minimum, which was 13.09 kN. But it was still larger than the specified minimum value of 12 kN
218 for the ballast in China’s high-speed railways with the design speed higher than 250 km/h [20]. It
219 means the lateral ballast resistances based on all the three new bonding schemes are adequate to

220 prevent the track from buckling.

221 Among the three bonding schemes, the maximum increment of the lateral resistance force was
222 observed when the ballast was reinforced at both areas near the sleeper ends and its centre due to
223 the largest bonding area in that case. In addition, comparing with the tests in which the bonding
224 depth was 200 mm, the lateral resistance force of the reinforced ballast with the bonding depth of
225 300 mm was larger by 14% when the ballast near the sleeper ends was reinforced, by 8% when the
226 ballast near the sleeper centre was reinforced and by 17% when the ballast at both areas was
227 reinforced. It can be concluded that the larger area and the larger thickness of ballast is reinforced
228 with the polyurethane, the larger lateral ballast resistance can be gained.

229 **4 Discrete element simulations on the lateral resistance of** 230 **polyurethane-reinforced ballast**

231 The DEM is a numerical method that excels in simulating the mechanical behaviours of the
232 granular material. It was firstly developed by Cundall and Strack [21] and has been successfully
233 applied to simulate the mechanical behaviours of railway ballast [22-27]. With the DEM, the
234 contact forces between granular particles and the particle movement can be simulated, which is
235 really helpful to investigate the micro-mechanical behaviours of the granular material.

236 The laboratory tests have shown distinct increase of the ballast resistance force when the ballast
237 is reinforced with the polyurethane. In order to reveal the micro mechanism that how the
238 polyurethane helps improve the lateral ballast resistance, the commercial DEM software Particle
239 Flow Code (PFC) was employed in this paper to simulate the SSPTs. The PFC deals with the
240 contact forces between particles based on the classic contact laws, and it calculates particle
241 movement according to Newton's Second Law [28]. It also provides bond models to simulate the
242 bonding behaviour between discrete particles, which can be used to simulate the bonding effect of

243 the polyurethane to the ballast particles. The DEM models that simulate the laboratory test track
244 including the polyurethane-reinforced ballast and the simulation results on the SSPTs will be
245 presented and discussed in this section.

246 *4.1 Discrete element modelling of ballast particles and polyurethane*

247 The ballast particles always have irregular shapes and angular corners since they are stones
248 mechanically crushed from intact rock. With the irregular shapes, the ballast particles interlock with
249 each other to keep the ballast stability after they are compacted in the track. To simulate the contact
250 and interlock behaviour between ballast particles well, discrete elements that can capture the
251 realistic ballast particle shapes are desirable for the DEM modelling. In this research, rigid clumps
252 with realistic particle shapes were generated with the laser scanning technique and the multi-sphere
253 overlapping algorithm to simulate the ballast particles. Similar methods can be found in Refs.
254 [26,29].

255 The procedures for generating the clumps are described here. First of all, three-dimensional
256 images of real ballast particles were obtained using a handheld laser scanner-FreeScan X3, as
257 shown in Fig. 7. Then, the images were imported into PFC to illustrate the particle surface, and the
258 volume enclosed by each particle surface was completely filled with several overlapping spheres.
259 Lastly, the irregular particle shape was approximated using a sufficient number of spheres with
260 different diameters, and these overlapping spheres were regarded as a clump in the DEM simulation.
261 In the present study, 20 real ballast particles with different shapes and size were scanned. Fig. 8
262 presents the different particle shapes and the corresponding clumps generated in PFC. The number
263 of the spheres composing each clump are also presented in the figure. Since there are a large
264 number of ballast particles in the test track, these clumps were repeatedly used for the DEM
265 modelling.

266 Utilizing the clumps, the contact behaviours between ballast particles were simulated with the
267 linear contact model which allowed sliding between the contacting clumps. Besides, in order to
268 simulate the ballast reinforced with the polyurethane, the bonding effects that the polyurethane
269 provided to the ballast particles were modelled by creating parallel bonds at the particle contact
270 points. When loading, these bonds can generate bond forces and moments to restrict the relative
271 movements of the contacting particles. The bond forces and moments were linearly determined by
272 the bond stiffness, the bond area and the particle relative movements according to the linear parallel
273 bond (LPB) model which was implemented in PFC. The details of the LPB model can be found in
274 the PFC manual [28]. Furthermore, the polyurethane material has a finite strength after enough
275 curing time and it may fracture when the reinforced ballast subjects to large external load. The
276 fracture behaviour of the polyurethane was also modelled with the LPB model. It means the parallel
277 bond breaks when the normal or shear stress on the bond induced by the bond forces and moments
278 exceeds the specified strength.

279 ***4.2 Discrete element simulations of SSPTs on ballast reinforced with polyurethane***

280 To simulate the SSPTs conducted in the laboratory, a 3D DEM model, as illustrated in Fig. 9a,
281 was firstly established to simulate the sleeper and the ballast in the test track without any
282 reinforcement. For the type IIIc sleeper, a stereo lithography (STL) file of the sleeper geometry was
283 generated in the software AutoCAD and imported into PFC. Then wall elements were generated to
284 reproduce the sleeper geometry. For the ballast, 45,355 clumps were generated according to the
285 particle size distribution of the ballast in laboratory tests and compacted to achieve a desirable
286 density. The side and base boundaries of the model were simulated using rigid wall elements. The
287 dimensions of the DEM model were consistent with the test track except that only one sleeper bay
288 was modelled here to reduce the simulation time while the laboratory test track has a total length of

289 12 m. In addition, after the DEM model was established, the sleeper was controlled to move down
290 according to the numerical servo mechanism in PFC^{3D} until the total vertical reaction force applied
291 to the sleeper base reached 2.7 kN which was equivalent to the weight of a real sleeper.

292 Based on this DEM model, parallel bonds were created to further simulate the ballast reinforced
293 with the polyurethane. Since not all the ballast particles were bonded with the polyurethane in the
294 laboratory tests, the parallel bonds were only created at the contacts between the ballast particles
295 that were located in the specified bonding region and depth according to each bonding scheme.
296 Thus, the DEM models in which the ballast particles in specified areas were bonded with the
297 parallel bonds were established to simulate the test tracks reinforced with the polyurethane to the
298 depth of 200 mm, as illustrated in Fig. 9.

299 The main parameters in the DEM models were listed in Table 4. The contact stiffness of the
300 particle-sleeper contacts were set much larger than that of the particle-particle contacts. It should be
301 pointed out that in the laboratory tests, the polyurethane material was manually sprayed from the
302 ballast top surface and automatically went down to the ballast voids due to its fluidity. Based on this
303 fact, it can be inferred that the bond effects of the polyurethane were uniform in the whole ballast
304 layer. Given the inhomogeneity of the bonding effects in the test track, the parallel bond stiffness
305 and strength in the DEM model were assumed to follow the Gaussian distribution. The mean value
306 of the normal bond strength was determined according the tensile strength of the polyurethane listed
307 in Table 1. For various bonding schemes, the same values of the micro-mechanical parameters were
308 used in the DEM models while the parallel bonds were created in different regions.

309 After the DEM models were established and cycled to equilibrium states, the simulations of the
310 SSPTs were performed by moving the sleeper along the lateral track direction at a speed of 4 mm/s.
311 This speed was set to be larger than that in the laboratory tests to save the computational time, and

312 the damping coefficient in the model was set to 0.5 to eliminate the dynamic effect due to the large
313 moving speed. The maximum lateral displacement was set to 3 mm because the laboratory test
314 results showed that the lateral resistance forces of the reinforced ballast were almost stable when the
315 lateral displacement exceeded 3 mm. During the simulations, the lateral displacement of the sleeper
316 and the lateral resistance force which was the lateral component of the sum of the contact forces
317 between the sleeper and ballast particles were monitored to investigate the lateral ballast resistance
318 responses.

319 *4.3 Validation of discrete element models*

320 Fig. 10 presents the simulation results of the lateral resistance force-displacement responses of
321 the reinforced ballast under various bonding schemes using the DEM models. The laboratory test
322 results were also presented in the figure for comparison. It can be seen that the DEM results have
323 good agreement with the test results when the sleeper displacement exceeds 2 mm, but there are
324 obvious differences between them in the initial phase. A possible reason for the difference is that the
325 large sleeper moving speed in the DEM simulations may result into reasonable dynamic effect to
326 the ballast which was not fully eliminated even though the global damping coefficient of 0.5 had
327 been considered. Meanwhile, the bonding behaviour of the polyurethane is quite complicated and
328 may have large variations under different conditions. Lacking of the knowledge on the micro
329 mechanical behaviours of the polyurethane bonds, a simple LPB model was adopted in the DEM
330 simulations. To better capture the responses in the initial phase, the particle contact behaviours and
331 the local bonding effects that the polyurethane applied to the ballast should be further investigated
332 in the future.

333 Overall, the DEM results exhibit similar increase trends and close stable values with the test
334 results for all the four bonding cases. When the lateral sleeper displacement reaches 2 mm, the

335 ballast resistance forces in the DEM results are 7.27, 14.30, 13.24 and 17.16 kN, respectively, for
336 the unreinforced ballast and that reinforced at the sleeper ends, centre and both areas. These values
337 are quite close to those measured in the tests as listed in Table 3. Hence, the established DEM
338 models for the unreinforced and reinforced ballast are reasonable and can reproduce the lateral
339 resistance force-displacement responses with good accuracy.

340 ***4.4 Micro-mechanical behaviour analysis***

341 In order to reveal the mechanism that how the polyurethane improves the ballast resistance, the
342 micro-mechanical behaviours of the ballast in the SSPTs are discussed hereinafter. According to the
343 DEM simulation results, the maximum particle displacement and distributions of the contact force
344 chains in the reinforced ballast are compared with those in the ordinary ballast without
345 reinforcement to show the restraints that the polyurethane provides to the ballast at the particle
346 scale.

347 Fig. 11 illustrates the force chain distributions in the ballast from different view angles when the
348 lateral sleeper displacement reaches 3 mm. In this figure, solid lines are plotted at the particle
349 contact points to represent the contact forces between ballast particles and those between the ballast
350 and the sleepers. Each line is orientated along the direction of the contact force it represents and its
351 thickness is proportional to the force magnitude. It can be observed that large contact forces are
352 generated near the sleeper end and diffused to the shoulder ballast to provide resistance to the
353 sleeper movement in all the four cases. For the ballasted track without the polyurethane, the
354 maximum contact force between the ballast and the sleeper end is 650 N. When the polyurethane is
355 applied to reinforce the ballast near the sleeper ends, near the sleeper centre and at both areas,
356 respectively, the maximum contact force increases to 1235.7 N, 976.4 N and 1561.9 N. The
357 maximum contact force increases by 90.1%, 50.2% and 1.4 times, respectively.

358 According to the DEM results, for the ballasted track without the polyurethane, the maximum
359 particle displacement is 3.13 mm when the lateral sleeper displacement d reaches 3 mm. When the
360 polyurethane is applied to reinforce the ballast near the sleeper ends, near the sleeper centre and at
361 both regions, the maximum particle displacement decreases to 2.91 mm, 2.98 mm and 2.84 mm,
362 respectively. The maximum particle displacement decreases by 7%, 4.8% and 9.3%, respectively.
363 Apparently, the maximum particle displacement of the ballast was restrained to a certain degree due
364 the bonding effect of the polyurethane to the ballast particles.

365 From the contact force chains and particle displacement results, it can be understood that the
366 polyurethane successfully restrains the ballast particle movement and improves the load-bearing
367 capacity of the granular ballast at the particle scale. This is because the polyurethane provides
368 strong bonding effect to the ballast particles so that effectively restrains the particle movement
369 induced by the squeezing and friction effect of the sleeper. With the large-area and effective
370 bonding of the polyurethane, the granular ballast particles are integrated to form a more stable
371 load-bearing structure. Hence, the polyurethane-reinforced ballast can provide larger resistance
372 force to the sleeper by restraining the particle movement inside it and increasing the contact force
373 network intensity.

374 **5 Conclusions**

375 This paper has proposed three new bonding schemes to reinforce the ballast with polyurethane more
376 efficiently by merely bonding the ballast near the sleeper ends or centre, or in both areas. Whereas
377 the shoulder ballast height is cancelled and the bonding area is small, the lateral resistance of the
378 polyurethane-reinforced ballast with the application of the new bonding schemes were investigated
379 in the paper.

380 A series of single sleeper pull-out tests were carried out to study the lateral resistance

381 force-displacement responses of the reinforced ballast. The test results indicated that if the ballast
382 was reinforced with polyurethane based on the proposed bonding schemes, the ballast resistance
383 was larger than that of the ordinary ballast without any reinforcement by at least 31%. These results
384 demonstrate that all the three new bonding schemes can ensure adequate ballast lateral resistance to
385 keep track stability.

386 Discrete element models were also established to simulate the SSPTs using clumps with realistic
387 particle shapes. Parallel bonds were created in the models to simulate the bonding effect of the
388 polyurethane to the ballast particles. The simulation results of the DEM models showed good
389 agreement with the laboratory test results. According to the DEM results, the particle displacement
390 and the contact force chains were analysed to investigate the micro-mechanical behaviours of the
391 reinforced ballast. It was found that the bonding effect of the polyurethane at the particle scale can
392 effectively restrain the movement of ballast particles and thereby successfully integrate the granular
393 ballast to form a more stable load-bearing structure, which provides larger ballast resistance force to
394 the sleeper than the ordinary granular ballast.

395 After the evaluation of ballast resistance in this study, the proposed bonding schemes have the
396 advantages of mitigating the ballast flight, saving the dosage of the polyurethane, having negligible
397 influence to the tamping operation and providing adequate ballast resistance simultaneously. These
398 bonding schemes can be chosen by engineers to mitigate the ballast flight risk in the high-speed
399 railways or to increase the ballast resistance effectively.

400 **Acknowledgements**

401 This work is supported by the Natural Science Foundation of China (NSFC) project under grant No. 51578051
402 and the Guangdong University of Technology Youth Fund under grant 18QNZD002.

403 **References**

- 404 [1] Esveld, C. (2001). *Modern railway track*, second edition. MRT-productions, The Netherlands.
- 405 [2] Esmaeili, M., Khodaverdian, A., Neyestanaki, H. K., & Nazari, S. (2016). Investigating the effect of nailed
406 sleepers, on increasing the lateral resistance of ballasted track. *Computers & Geotechnics*, 71, 1-11.
- 407 [3] Esmaeili, M., Zakeri, J. A., & Babaei, M. (2017). Laboratory and field investigation of the effect of
408 geogrid-reinforced ballast on railway track lateral resistance. *Geotextiles & Geomembranes*, 45(2), 23-33.
- 409 [4] Kasraei, A., Zakeri, J. A., Esmaeili, M., & Bakhtiary, A. (2016). A numerical investigation on the lateral
410 resistance of frictional sleepers in ballasted railway tracks. *Proceedings of the Institution of Mechanical
411 Engineers, Part F: Journal of Rail & Rapid Transit*, 10(6), 1-10.
- 412 [5] Koike, Y., Nakamura, T., Hayano, K., & Momoya, Y. (2014). Numerical method for evaluating the lateral
413 resistance of sleepers in ballasted tracks. *Soils & Foundations*, 54(3), 502-514.
- 414 [6] Tutumluer, E., Huang, H., Hashash, Y., and Ghaboussi, J. (2006). Aggregate shape effects on ballast tamping
415 and railroad track lateral stability. *Proc., Annual Conf. of the American Railway Engineering and
416 Maintenance-of-Way Association, American Railway Engineering and Maintenance-of-Way Association,
417 Lanham, MD.*
- 418 [7] Quinn, A. D., Hayward, M., Baker, C. J., Schmid, F., Priest, J. A., & Powrie, W. (2010). A full-scale
419 experimental and modelling study of ballast flight under high-speed trains. *Proceedings of the Institution of
420 Mechanical Engineers, Part F: Journal of Rail & Rapid Transit*, 224(2), 61-74.
- 421 [8] Premoli, A., Rocchi, D., Schito, P., Somaschini, C., & Tomasini, G. (2015). Ballast flight under high-speed
422 trains: wind tunnel full-scale experimental tests. *Journal of Wind Engineering & Industrial Aerodynamics*, 145,
423 351-361.
- 424 [9] Jönsson, M., Ehrenfried, K., Loose, S., & Wagner, C. (2014). Particle image velocimetry of the underfloor
425 flow of generic high-speed train models in a water towing tank. *Proceedings of the Institution of Mechanical
426 Engineers, Part F: Journal of Rail & Rapid Transit*, 228(2), 194-209.

- 427 [10] Goo, J. S., Kim, J. S., & Shin, K. B. (2015). Evaluation of structural integrity after ballast-flying impact
428 damage of a grip lightweight bogie frame for railway vehicles. *Journal of Mechanical Science & Technology*,
429 29(6), 2349-2356.
- 430 [11] Le Pen, L., & Powrie, W. (2011). Contribution of base, crib, and shoulder ballast to the lateral sliding
431 resistance of railway track: a geotechnical perspective. *Proceedings of the Institution of Mechanical Engineers*,
432 Part F: *Journal of Rail & Rapid Transit*, 225(2), 113-128.
- 433 [12] Lee S. H., Lee, S. J., Park, J. G., & Choi, Y. T. (2017). An experimental study on the characteristics of
434 polyurethane-mixed coarse aggregates by large-scale triaxial test. *Construction & Building Materials*, 145,
435 117-125.
- 436 [13] Woodward, P. K., Kacimi, A. E., Laghrouche, O., Medero, G., & Banimahd, M. (2012). Application of
437 polyurethane geocomposites to help maintain track geometry for high-speed ballasted railway tracks. *Journal*
438 *of Zhejiang University-Science A (Applied Physics & Engineering)*, 13(11), 836-849.
- 439 [14] Woodward, P. K., Kennedy, J., Medero, G. M., & Banimahd, M. (2012). Maintaining absolute clearances in
440 ballasted railway tracks using in situ three-dimensional polyurethane geocomposites. *Proceedings of the*
441 *Institution of Mechanical Engineers, Part F: Journal of Rail & Rapid Transit*, 226(226), 257-271.
- 442 [15] Woodward, P. K., Kennedy, J., Laghrouche, O., Connolly, D. P., & Medero, G. (2014). Study of railway track
443 stiffness modification by polyurethane reinforcement of the ballast. *Transportation Geotechnics*, 1(4),
444 214-224.
- 445 [16] Kennedy, J., Woodward, P. K., Medero, G., & Banimahd, M. (2013). Reducing railway track settlement using
446 three-dimensional polyurethane polymer reinforcement of the ballast. *Construction & Building Materials*,
447 44(3), 615-625.
- 448 [17] Woodward, P. K., Kennedy, J., Medero, G. M., & Banimahd, M. (2012). Application of in situ polyurethane
449 geocomposite beams to improve the passive shoulder resistance of railway track. *Proceedings of the*

- 450 Institution of Mechanical Engineers, Part F: Journal of Rail & Rapid Transit, 226(3), 294-304.
- 451 [18] Kruglikov, A. A. Yavna, V. A. & Ermolov, Y. M. (2017). Strengthening of the railway ballast section shoulder
452 with two-component polymeric binders. *Transportation Geotechnics*, 11: 133-143.
- 453 [19] Thomas, S., Woodward, P., & Laghrouche, O. (2015). Influence of stiffening ballasted track bed overlying a
454 masonry arch bridge using a polyurethane polymer material. *Construction & Building Materials*, 92, 111-117.
- 455 [20] National Railway Administration of P.R. China. (2014). Code for design of high speed railways. China
456 Railway Press, Beijing. (in Chinese)
- 457 [21] Cundall, P. A., & Strack, O. D. L. (1979). A discrete numerical model for granular assemblies. *Geotechnique*,
458 29(30), 331-336.
- 459 [22] Chen, C., Mcdowell, G. R., and Thom, N. H. (2012). Discrete element modelling of cyclic loads of
460 geogrid-reinforced ballast under confined and unconfined conditions. *Geotextiles and Geomembranes*,
461 35(35):76-86.
- 462 [23] Indraratna, B., Ngo, N. T., Rujikiatkamjorn, C., and Vinod, J. S. (2012). Behaviour of fresh and fouled
463 railway ballast subjected to direct shear testing: discrete element simulation. *International Journal of*
464 *Geomechanics*, 14(1):34-44.
- 465 [24] Tutumluer, E., Qian, Y., Hashash, Y. M. A., Ghaboussi, J., and Davis, D. D. (2013). Discrete element
466 modelling of ballasted track deformation behaviour. *International Journal of Rail Transportation*, 1(1-2):57-73.
- 467 [25] Zhang, X., Zhao, C., & Zhai, W. (2017). Dynamic behavior analysis of high-speed railway ballast under
468 moving vehicle loads using discrete element method. *International Journal of Geomechanics*, 17(7):
469 04016157.
- 470 [26] Zhang X., Zhao C. & Zhai W. (2019). Importance of load frequency in applying cyclic loads to investigate
471 ballast deformation under high-speed train loads. *Soil Dynamics and Earthquake Engineering*, 120:28-38.
- 472 [27] Ling, X., Xiao, H., & Cui, X. (2018). Analysis of mechanical properties of polyurethane-mixed ballast based

- 473 on energy method. *Construction & Building Materials*, 182, 10-19.
- 474 [28] Itasca Consulting Group. (2008). Particle flow code in three dimensions (PFC3D), Minneapolis.
- 475 [29] Anochie-Boateng, J. K., Komba, J. J., & Mvelase, G. M. (2013). Three-dimensional laser scanning technique
- 476 to quantify aggregate and ballast shape properties. *Construction & Building Materials*, 43(43), 389-398.

477 **Table list:**

478 Table 1 Mechanical properties of the polyurethane used in the test

Parameter	Value
Density (g/cm ³)	1.13
Tensile strength (MPa)	14.2
Elongation at break (%)	20
Tearing strength (N/mm)	60
Shore hardness	46

479

480 Table 2 Summary of the tests carried out in the laboratory

Test name	Shoulder height (mm)	Bonding area	Bonding depth from the top surface (mm)
Ns	150	None	0
Nf	0	None	0
E2	0	At sleeper ends	200
E3	0	At sleeper ends	300
C2	0	near sleeper center	200
C3	0	near sleeper center	300
B2	0	both areas	200
B3	0	both areas	300

481

482

483

Table 3 Lateral resistance forces of ballast at $d=2\text{mm}$ in various tests and their differences

Test	Lateral resistance force (kN)	Difference from Ns	Difference from Nf
Ns	10.0	-	42%
Nf	7.05	-30%	-
E2	14.09	41%	100%
E3	16.07	60%	128%
C2	13.09	31%	86%
C3	14.09	41%	100%
B2	17.08	70%	142%
B3	20.02	100%	184%

484

485

486

Table 4 The micro-mechanical parameters in the DEM simulations

Parameters	Value	Parameters	Mean value	Standard error
Damping coefficient	0.5	Parallel bonds		
Ballast particles		Normal stiffness (N/m^2)	1.5×10^7	1.0×10^6
Clump density (kg/m^3)	2700	Shear stiffness (N/m^2)	1.5×10^7	1.0×10^6
Normal stiffness (N/m)	1×10^8	Tensile strength (Pa)	1.42×10^7	1.0×10^6
Shear stiffness (N/m)	1×10^8	Cohesive strength (Pa)	1.42×10^7	1.0×10^6
Friction coefficient	0.5	Friction angle ($^\circ$)	45	0
Ballast-sleeper contacts				
Normal stiffness (N/m)	5×10^9			
Shear stiffness (N/m)	5×10^9			
Friction coefficient	0.5			

487

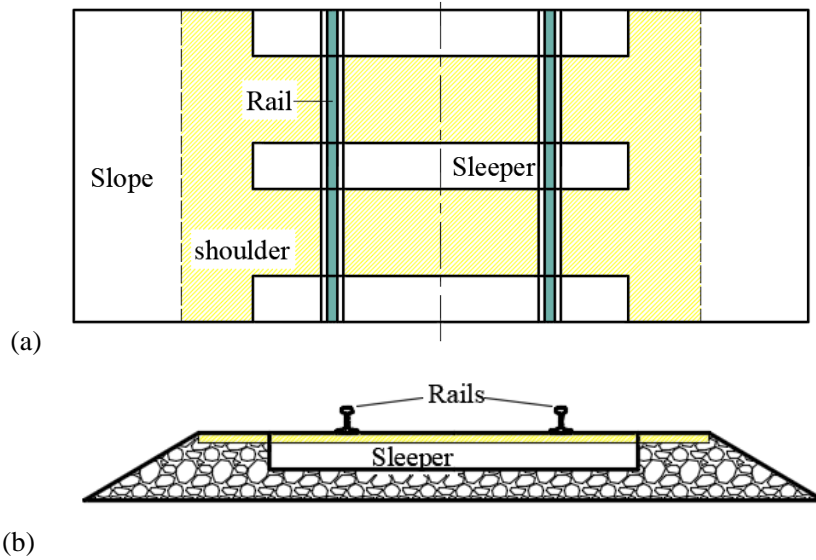


Fig. 1 Sketch of the target region (in yellow) in the conventional bonding scheme for reinforcing the ballast with polyurethane: (a) plane view and (b) end view

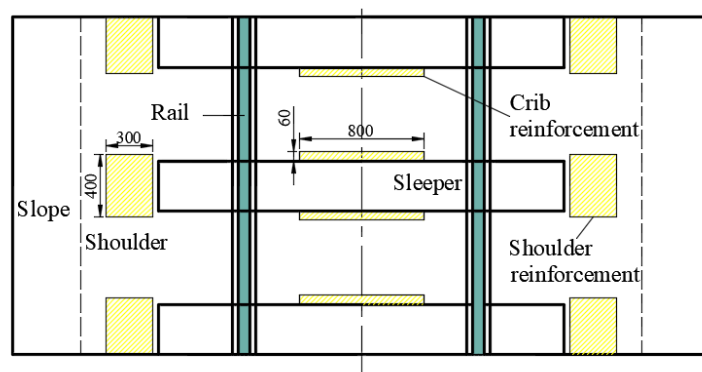


Fig. 2 Sketch of the target regions (in yellow) in the new bonding schemes for reinforcing the ballast with polyurethane (unit: mm)

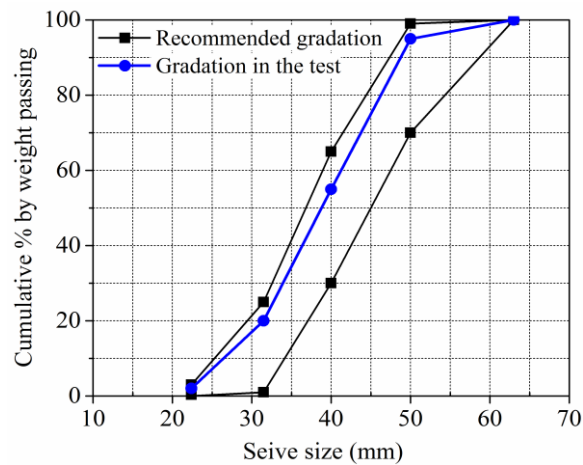


Fig. 3 Particle size gradation of ballast in the tests

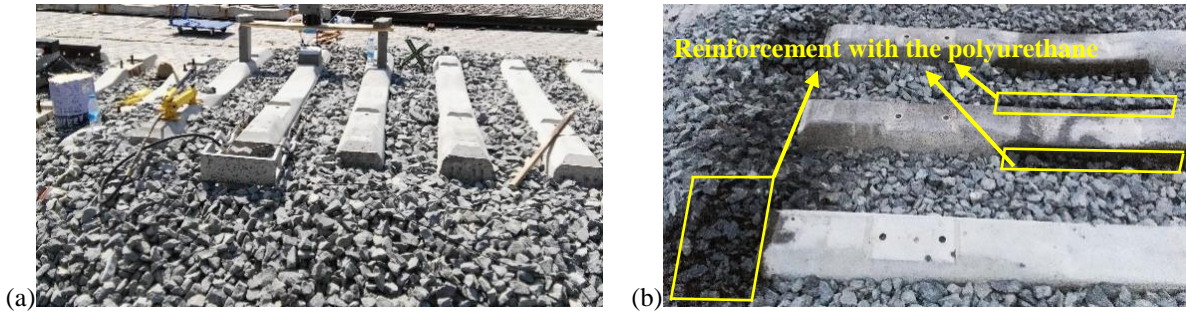


Fig. 4 Photographs of the ballasted track with and without the reinforcement of the polyurethane: (a) without reinforcement, (b) reinforced at both regions

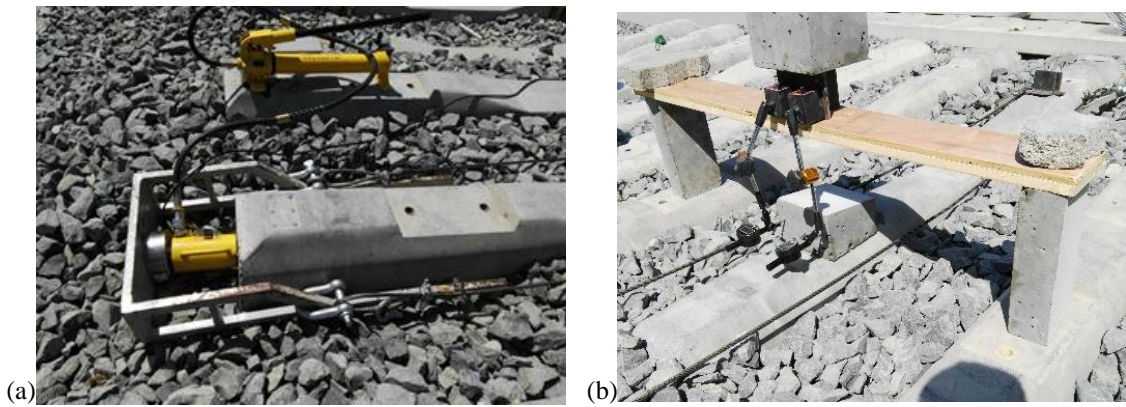


Fig. 5 Apparatus for measuring (a) the lateral resistance force of the ballast and (b) the lateral displacement of the sleeper

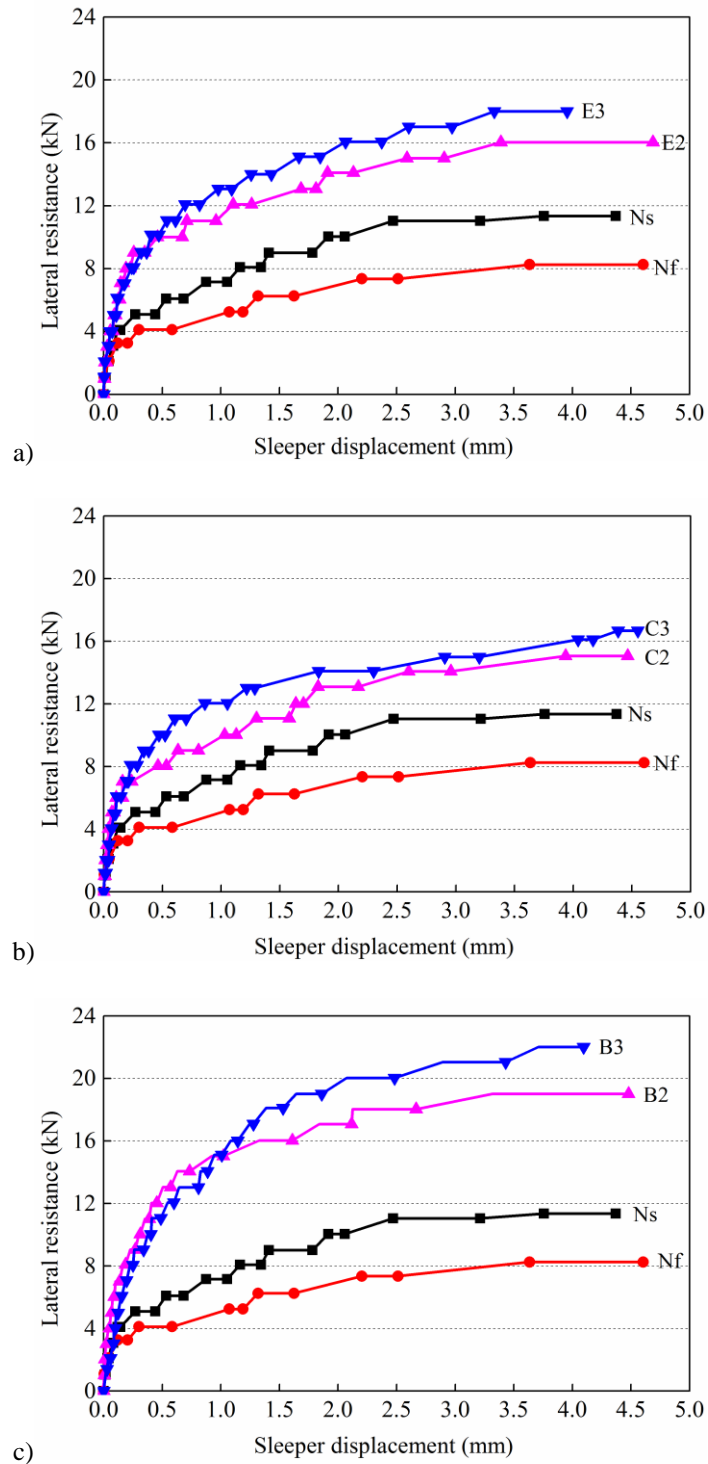


Fig. 6 Test results of the lateral resistance force-displacement responses of the reinforced ballast based on various bonding schemes: (a) reinforced near the sleeper ends, (b) reinforced near the sleeper centre and (c) reinforced at both regions

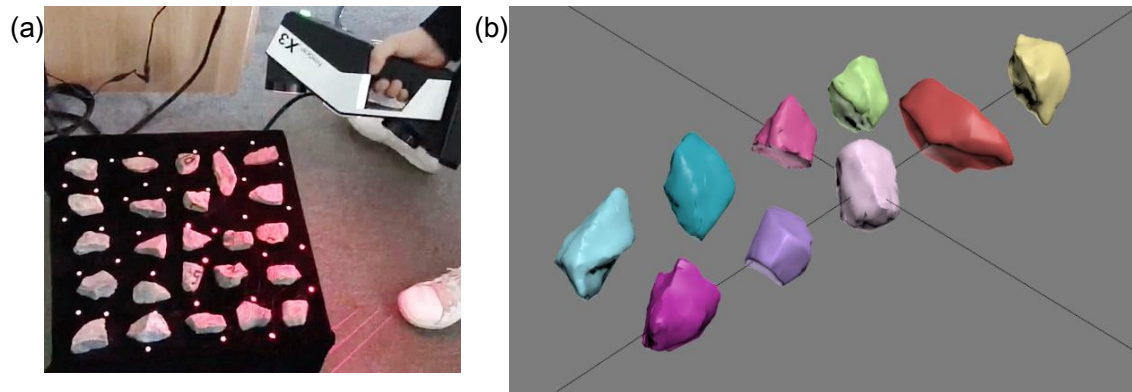


Fig. 7 3D laser scanning of ballast particles: (a) photograph of scanning and (b) the scanned images

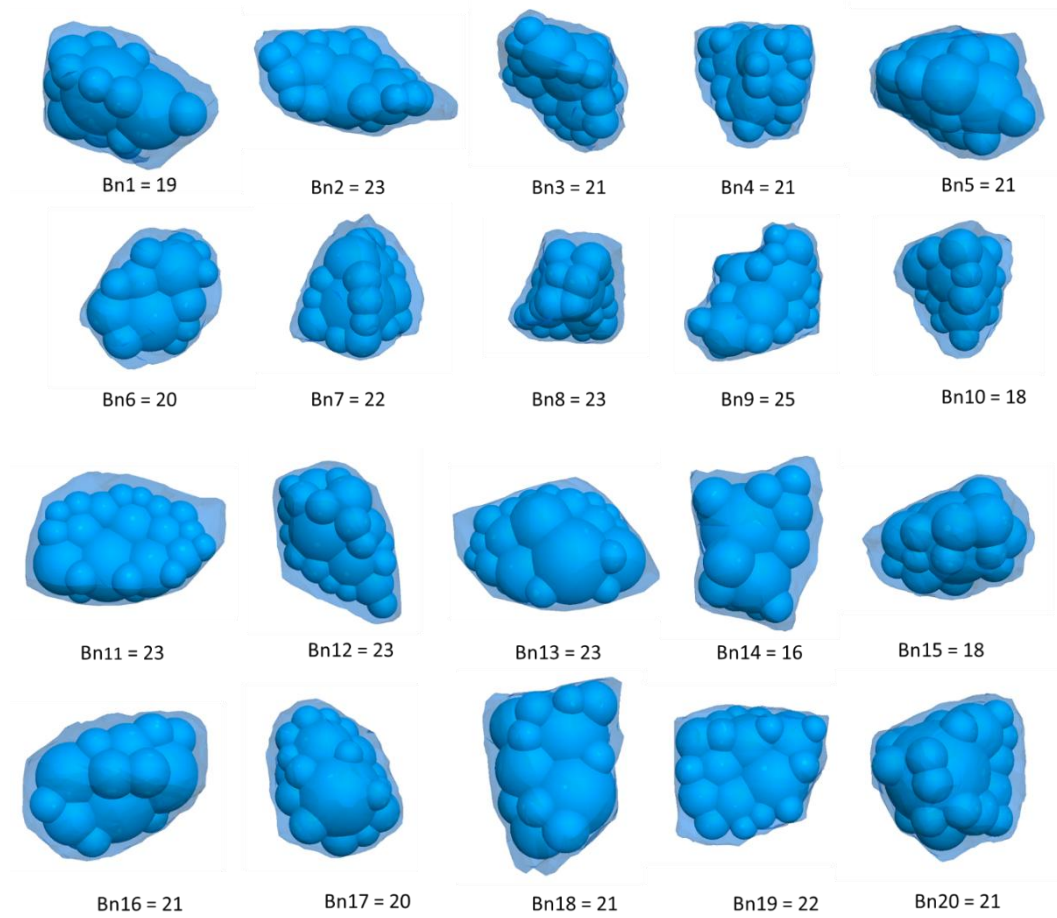


Fig. 8 Ballast particle shapes and clumps generated in PFC

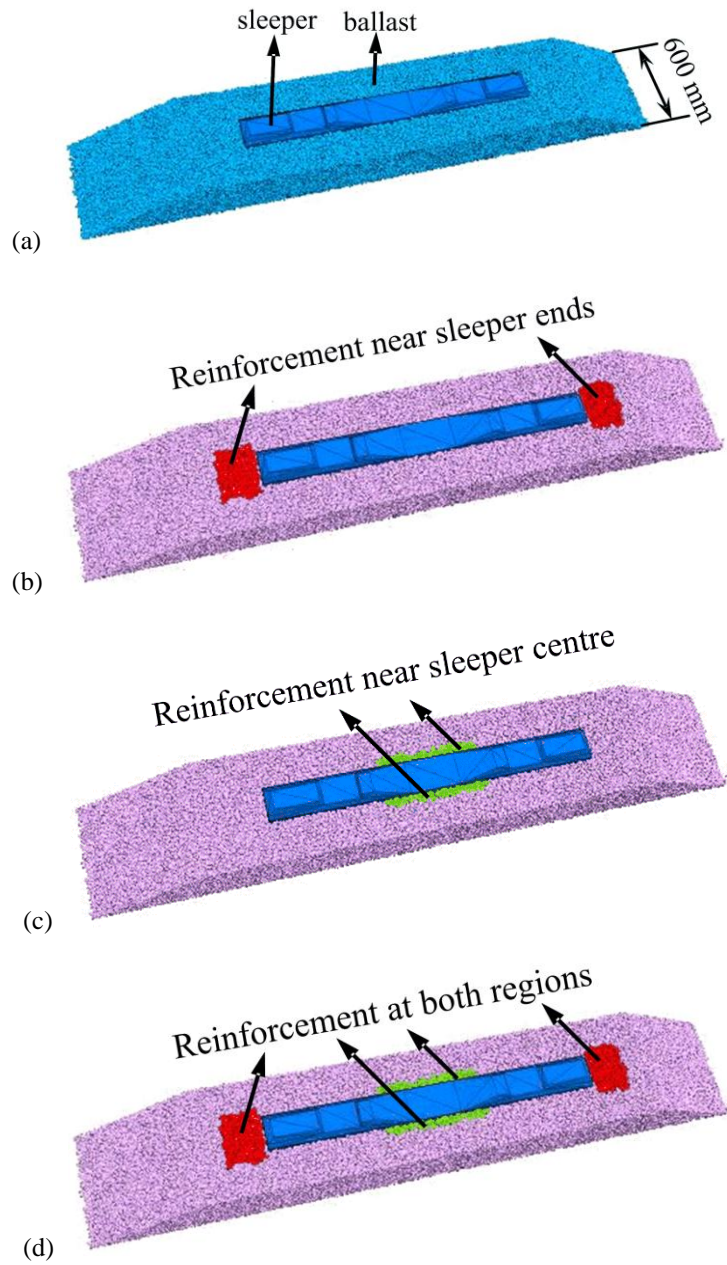


Fig. 9 The DEM models of the sleeper-ballast structure with and without the reinforcement of polyurethane: (a)without reinforcement, (b)reinforced near the sleeper ends, (c)reinforced near the sleeper centre and (d)reinforced at both regions

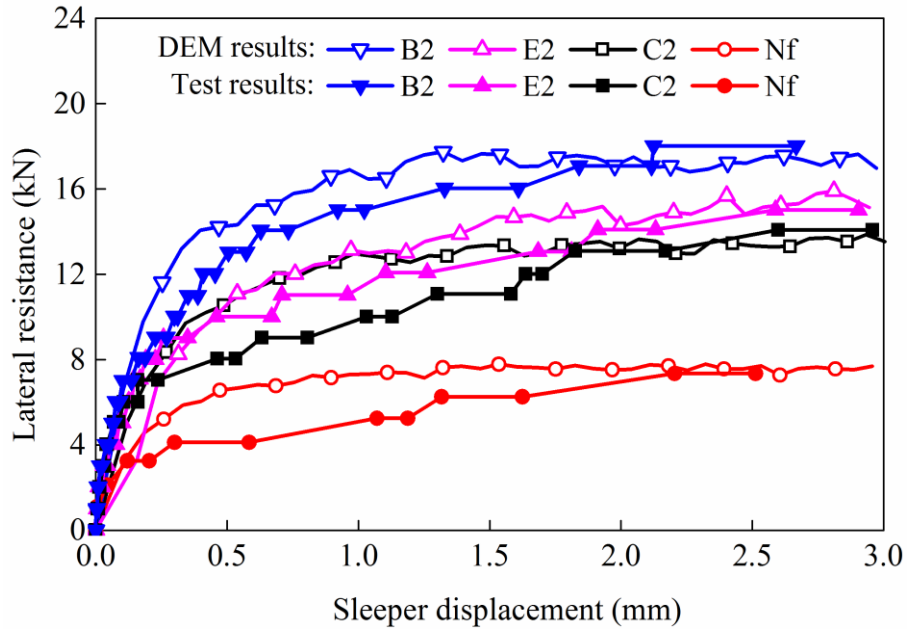


Fig.10 The resistance force-displacement responses of the reinforced ballast: a comparison between the DEM and test results

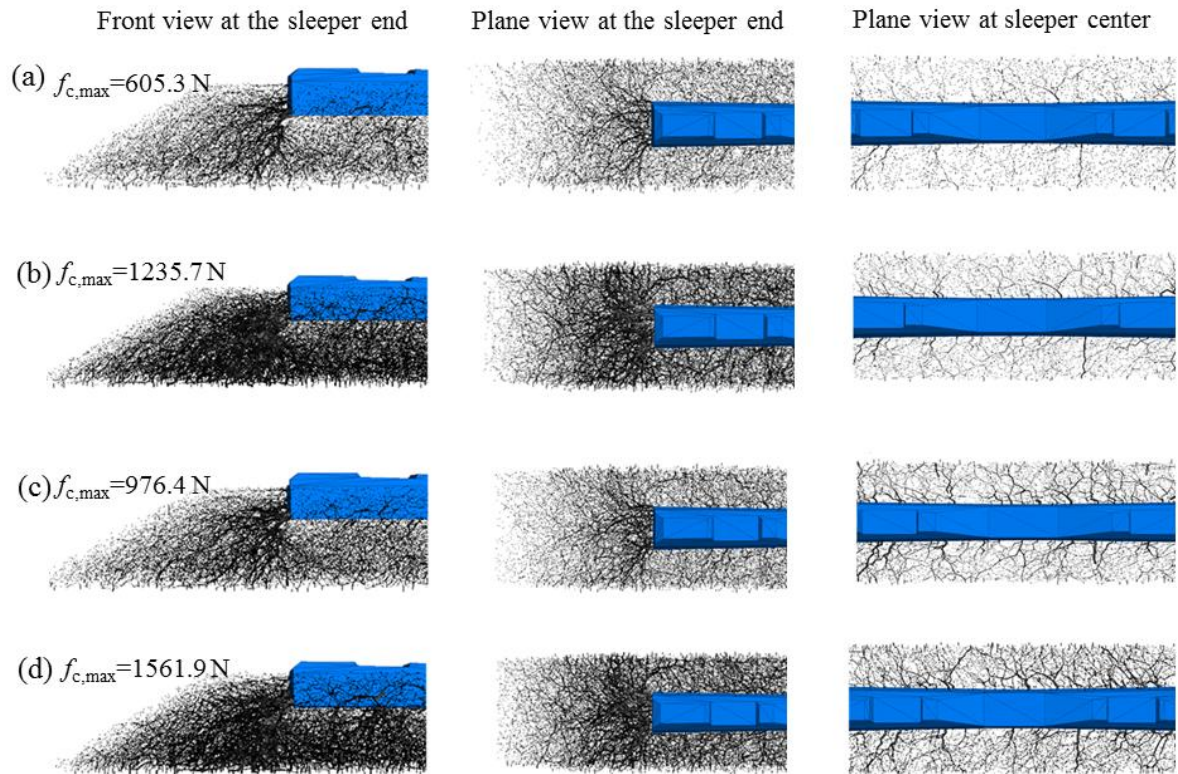


Fig.11 Contact force chains distributions in the ballast at $d=3\text{mm}$: (a) unreinforced ballast, (b) reinforced near the sleeper ends, (c) reinforced near the sleeper center and (d) reinforced at both regions